Process Development for Electron Beam Melting of 316LN Stainless Steel

Stefan Roos

Main supervisor: Lars-Erik Rännar
Co-supervisors: Andrei Koptioug, Jonas Danvind

Sports Tech Research Centre
Department of Quality Management and Mechanical Engineering (KMT)
Faculty of Science, Technology and Media
Thesis for Degree of Licentiate of Technology
Mid Sweden University
Östersund, 2019-12-18

Akademisk avhandling som med tillstånd av Mittuniversitetet i Östersund framläggs till offentlig granskning för avläggande av teknologie licentiatexamen Onsdag, 2019-12-18, 9:00, Q221, Mittuniversitetet Östersund. Seminariet kommer att hållas på svenska

Process Development for Electron Beam Melting of 316LN Stainless Steel

Printed by Mid Sweden University, Sundsvall
ISSN: 1652-8948
ISBN: 978-91-88947-25-3

Faculty of Science, Technology and Media
Mid Sweden University, SE-831 25, Östersund
Phone: +46 (0)10 142 80 00
Mid Sweden University Licentiate Thesis 164

To my family

Acknowledgements

I would like to acknowledge my supervisors — Lars-Erik Rännar, Andrei Koptioug, and Jonas Danvind — for their input and for our discussions about both this thesis and the research described here. I would also like to thank Per Skoglund for help and discussion regarding the operation and functionality of the EBM machines, and Carlos Botero, William Sjöström, and Magnus Hummelgård for help and discussion regarding the characterization of samples and material principles. Finally, thanks go to everyone else who has contributed to this thesis in some way.

Table of contents

Abstract

Title: Process Development for Electron Beam Melting of 316LN Stainless Steel

Keywords: additive manufacturing, beam deflection rate, electron beam melting, energy input, material properties, microstructure, powder bed fusion, process parameters, 316LN stainless steel

ISBN:

Additive manufacturing (AM) is a technology that inverts the procedure of traditional machining. Instead of starting with a billet of material and removing unwanted parts, the AM manufacturing process starts with an empty workspace and proceeds to fill this workspace with material where it is desired, often in a layer-by-layer fashion. Materials available for AM processing include polymers, concrete, metals, ceramics, paper, photopolymers, and resins. This thesis is concerned with electron beam melting (EBM), which is a powder bed fusion technology that uses an electron beam to selectively melt a feedstock of fine powder to form geometries based on a computer-aided design file input. There are significant differences between EBM and conventional machining. Apart from the process differences, the ability to manufacture extremely complex parts almost as easily as a square block of material gives engineers the freedom to disregard complexity as a cost-driving factor. The engineering benefits of AM also include manufacturing geometries which were previously almost impossible, such as curved internal channels and complex lattice structures. Lattices are lightweight structures comprising a network of thin beams built up by multiplication of a three-dimensional template cell, or unit cell. By altering the dimensions and type of the unit cell, one can tailor the properties of the lattice to give it the desired behavior. Lattices can be made stiff or elastic, brittle or ductile, and even anisotropic, with different properties in different directions. This thesis focuses on alleviating one of the problems with EBM and AM, namely the relatively few materials available for processing. The method is to take a closer look at the widely used stainless steel 316LN, and investigate the possibility of processing 316LN powder via the EBM process into both lattices and solid material. The results show that 316LN is suitable for EBM processing, and a processing window is presented. The results also show that some additional work is needed to optimize the process parameters for increased tensile strength if the EBM-processed material is to match the yield strength of additively laser-processed 316L material.

Sammanfattning

Additiv tillverkning (förkortas AM som i det engelska *Additive Manufacturing*) är en teknologi som omkastar tillvägagångssättet med vanlig maskinbearbetning. Traditionell maskinbearbetning utgår från ett ämne av valt material, från ämnet bearbetas det som inte behövs bort. AM utgår från ett tomt arbetsbord och fyller sedan bordet med det material som senare blir den färdiga parten, ofta genom påbyggnad lager för lager. Exempel på material som idag finns tillgängliga för AM inkluderar plaster, betong, metaller, keramer, papper, fotopolymerer och hartser. För de artiklar som inkluderas i denna avhandling har elektronstrålesmältning använts. Elektronstrålesmältning är en pulverbäddsteknologi, vilket innebär att ett fint pulver används som råmaterial. En elektronstråle smälter utvalda delar av pulvret för att forma geometrier baserade på en datorstödd modelleringsfil. Jämför man elektronstrålesmältning med traditionell maskinbearbetning finns det signifikanta skillnader. Bortsett från rena processkillnader ger elektronstrålesmältning möjligheten att tillverka extremt komplexa geometrier nästan lika lätt som ett simpelt rätblock vilket ger ingenjörer möjligheten att bortse från en parts komplexitet som kostdrivande under designarbetet. Ingenjörer får genom AM också möjligheten att använda geometrier som tidigare ansågs mer eller mindre omöjliga att tillverka, t.ex. krökta interna kanaler. Fackverk är lättviktskonstruktioner bestående av tunna balkar. En nedbrytning av en fackverkskonstruktion visar att den är uppbyggd genom multiplicering av en tredimensionell mall-cell, en så kallad enhetscell. Genom att ändra dimensionerna på, och typ av, enhetscell kan fackverkets egenskaper skräddarsys för att bete sig enligt behov. Fackverken kan t.ex. vara styva eller elastiska, sköra eller sega och till och med anisotropiska, vilket innebär olika egenskaper i olika riktningar. Denna avhandling fokuserar på att ge ett bidrag till ett av elektronstrålesmältnings och AMs utmaningar; det finns för få material tillgängliga för tekniken. Metoden som använts har varit att undersöka om det rostfria stålet 316LN, ett välkänt och välanvänt material inom industrin, är lämpligt och möjligt att processa via EBM till både fackverk och solida strukturer. Resultatet visar att 316LN är lämpligt för EBM-processen och i avhandlingen presenteras ett processfönster. Resultaten visar också att en del arbete kvarstår i optimeringen av processparametrar för ökad sträckgräns om EBM-processat material ska kunna nå samma egenskaper som material processat med laserbaserade metoder.

List of papers

This thesis is based primarily on the following three papers:

Paper I *Characterization of 316LN lattice structures fabricated via electron beam melting*

S. Roos, L.-E. Rännar, A. Koptioug, J. Danvind

Materials Science and Technology Conference and Exhibition 2017 (MS&T17), Association for Iron and Steel Technology (2017), 336–343.

Author contribution: As the first author, Stefan Roos designed the experiments, fabricated all the lattice samples, and carried out most of the characterization.

Paper II *Macro- and micro mechanical behavior of 316LN lattice structures manufactured by electron beam melting*

S. Roos, C. Botero, J. Danvind, A. Koptioug, L.-E. Rännar
Accepted for publication in the *Journal of Materials Engineering and Performance*.
Author contribution: As the first author, Stefan Roos designed the study, manufactured all the samples, and performed all the characterization and writing except the work with nanoindentation.

Paper III *Process window for electron beam melting of 316LN stainless steel*

S. Roos

Submitted for review.

Author contribution: As the single author, Stefan Roos was responsible for all the work and writing involved in this study.

The co-authors' contributions to these papers included project facilitation in the form of financial management, requisition of materials, pre-editing papers, and supplying a knowledgeable environment in which ideas could be discussed, evaluated, and improved.

Related publications not included in this thesis:

Paper A *Nanoindentation: a suitable tool in metal Additive Manufacturing.*

C.A. Botero Vega, E. Jiménez-Piqué, S. Roos, P. Skoglund, A. Koptioug, L. Rännar, M. Bäckström

Presented at the Materials Science and Technology Conference and Exhibition 2018 (MS&T18), 14–18 October 2018, Columbus, USA.

Definitions and abbreviations

AM: additive manufacturing

ASTM: American Society for Testing and Materials (an international standards organization)

ASTM A240: Standard specification for chromium and chromium-nickel stainless steel plate, sheet, and strip for pressure vessels and for general applications

CAD: computer-aided design

DMD: direct metal deposition

DMLS: direct metal laser sintering

EBDM: electron beam direct manufacturing

EBM: electron beam melting

EB-PBF: electron beam powder bed fusion

EDS: energy-dispersive x-ray spectroscopy

IFF: ion fusion formation

L-PBF: laser powder bed fusion

LC: laser cladding

LD: laser deposition

LENS: laser engineered net shaping

Part: an object fabricated using AM

PBF: powder bed fusion

PTAS FFF: plasma transferred arc selected free form fabrication

SEM: scanning electron microscope

SLM: selective laser melting

Ti6Al4V: titanium 6-aluminium 4-vanadium (a titanium alloy)

1 Introduction

There are many different forms of manufacturing, and even more designations and trade names, for what has lately been gathered under the collective name of additive manufacturing (AM). The American Society for Testing and Materials (ASTM) defines AM as:

"A process of joining materials to make parts from 3D model data, usually layer upon layer, as opposed to subtractive manufacturing and formative manufacturing methodologies. Historical terms: additive fabrication, additive processes, additive techniques, additive layer manufacturing, solid freeform fabrication and freeform fabrication". [1]

All additive manufacturing methods start from an empty workspace and build up the desired object, but they differ in their methods of joining material together. Depending on one's definition, the history of AM dates back over 150 years. In 1860, an artist named François Willème arranged a series of cameras in a circular pattern around an object. The resulting photos were used to carve cylindrical portions of the photographed object, and a "3D photograph" was created. In 1892, Blanter [2] patented a method for stacking a series of wax plates, called "contour relief maps", with carved out contours in them to create molds for making paper relief maps. Even though these pioneers of the technology may be called the inventors of AM and 3D modeling, their methods have little in common with AM as we see it today.

The introduction of modern AM is often symbolized by stereolithography [3], which was originally proposed by Munz [4] in 1951. Munz's system was based on selective solidification of a layer of photopolymer, using a piston mechanism that continuously lowered a build platform while new photopolymer was added to the top, thus building an object. In 1968, Swainson [5] proposed a refinement of Munz's system by adding a laser beam to selectively solidify the photopolymer. The use of powders for AM was first introduced in 1971 by Ciraud [6], who used laser, electron, and plasma beams to partially melt powder. By the early 1980s AM technology was rapidly moving forward, with 1981–1982 seeing the earliest powder laser sintering process [7], the first rapid prototyping system that used functional photopolymers [8], and a system that used a computer to control the laser beam of a stereolithography system [9]. The term "3D printing", which is sometimes used instead of "additive manufacturing", in fact refers to a subcategory of AM developed at the Massachusetts Institute of Technology in the 1980s. Substantial diversification took place in the late 1980s and 1990s,

with numerous new technologies being introduced and companies being formed to commercialize AM. Nevertheless, the breakthrough of AM still took another decade, and even then AM was primarily used for prototyping and visualization. Today, many AM technologies are widespread, and one can buy a fused deposition modeling polymer machine for home use for less than 150 USD. However, a professional powder bed fusion (PBF) polymer machine is still in the range of 100 000 USD upwards.

Figure 1 shows a typical AM workflow from the computer-aided design (CAD) model to the finished product. The work begins by creating a 3D model which describes the desired final product. This model is then sliced into layers using software that allows machine-specific code to be generated. A feedstock appropriate for the chosen AM technology (wire, powder, etc.) is used for the manufacturing process. Technology-dependent post-processing is often required after manufacturing; for stereolithography this could be post-curing of resin, for PBF it could be powder removal, and for almost all processes some type of support structure removal is necessary.

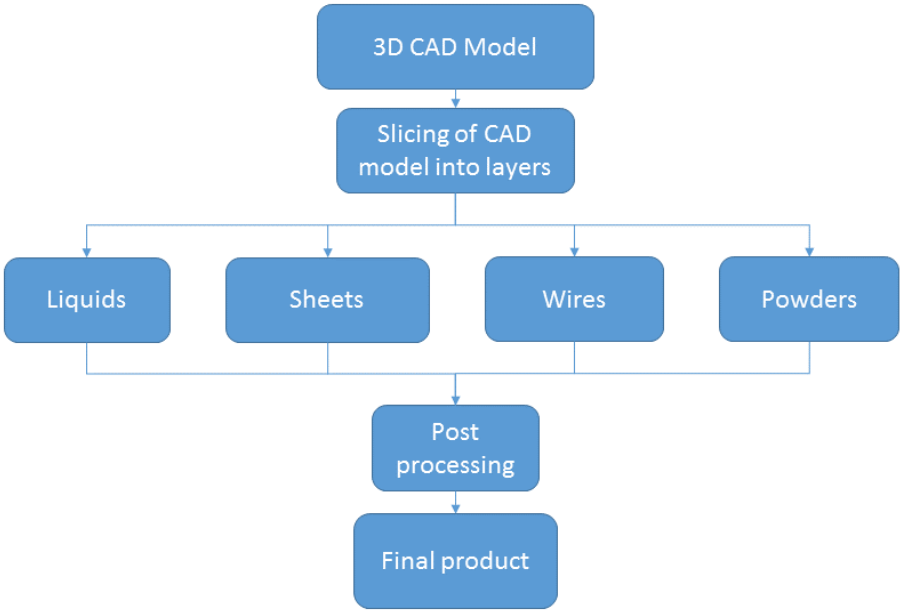

Figure 1. Typical AM workflow from CAD model to finished product.

One of the advantages of AM over traditional manufacturing lies in the fact that complex shapes do not directly drive cost; in general, building a complex lattice structure is no more expensive than building a rectangular block.

Another is the ability to manufacture parts with geometries complex enough that AM is the only viable option, such as curved internal channels for coolant, and complex lattice structures. Further advantages of AM include the following:

- Consolidation of parts: Instead of creating multiple parts and joining them together, several parts can be built as one, which can reduce complexity and increase production efficiency
- Ease of creating a revision: If a part needs a revision or if several varieties need to be made, no tooling needs to be altered, only the CAD file.
- Individual adaptation: Building 100 individually-adapted medical implants is just as easy as building 100 identical ones, though build preparation is likely more complex.
- Almost no limitations: Even if AM is not limit-free, the limitations are relatively few and almost any geometry can be built.
- Short lead-time: Since AM is tooling-free, the process is ready to start shortly after the CAD model has been finalized. In research and development, this means prototypes are ready for testing within days or even hours, rather than the weeks they could take if there is a need for specific tooling.

These examples show how AM can be competitive in comparison with conventional methods, but one should remember that AM technology will never become the only solution for manufacturing. There will always exist products that are more suitable for traditional manufacturing.

AM is becoming more accepted industrially, as standardization of methods/processes and knowledge of the technology increases. However, there is still some way to go before a major breakthrough. For AM as a whole, one challenge is the blessing and curse of how the combination of process parameters and part geometry influences the material properties of the final parts. For Electron beam powder bed fusion (EB-PBF) specifically, there is the challenge of the low number of materials available for processing; EB-PBF has only six materials available, while laser-based powder bed fusion (L-PBF) has approximately 25–30.

2 Objectives

This thesis for the degree of Licentiate of Technology aims to investigate the possibility of adapting the Electron beam melting (EBM) process to successfully fabricate high quality parts using stainless steel 316LN precursor powder. This requires examination of the relationship between the process parameters and the mechanical and microstructural properties of the final material. The overall goal is to provide a processing window that allows solid parts to be fabricated with a high build rate while maintaining the desired mechanical and microstructural properties.

The following research questions are addressed in order to meet the stated objectives:

- RQ1: Is it possible to use EBM to fabricate lightweight structures in stainless steel 316LN?
- RQ2: How does energy input affect the mechanical and microstructural properties of EBM-fabricated lightweight structures in 316LN stainless steel?
- RQ3: What are the mechanical and microstructural properties of bulk stainless steel 316LN processed via EBM using different process parameters within a relevant process window?

The methodology used to address the objectives is depicted in Figure 2 as a schematic flowchart describing the different steps in the process development. This thesis covers all the steps, whereas most attention is paid to the EBM processing and characterization of the manufactured specimens.

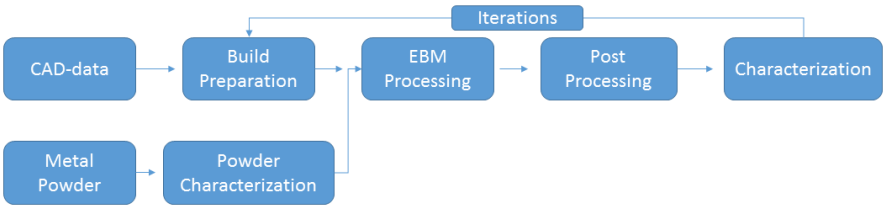

Figure 2. Flowchart describing the EBM process development procedure used for studies of 316LN stainless steel.

3 Metal additive manufacturing

Metal AM partly, or completely, fuses metal together utilizing a heat source. This sets metal AM apart from other types of AM that rely on stacking sheets or chemical hardening. Three main types of heat sources are used: laser beam, electron beam, and plasma (arc). There are also three main types of feedstock: powder bed, powder feed, and wire feed. Laser beam and electron beam can be used with all forms of feedstock, while plasma is mainly used with wire feed [10]. Figure 3 shows a hierarchical chart of metal AM as well as some trade/process names under each category. This thesis focuses on powder bed fusion using an electron beam as heat source.

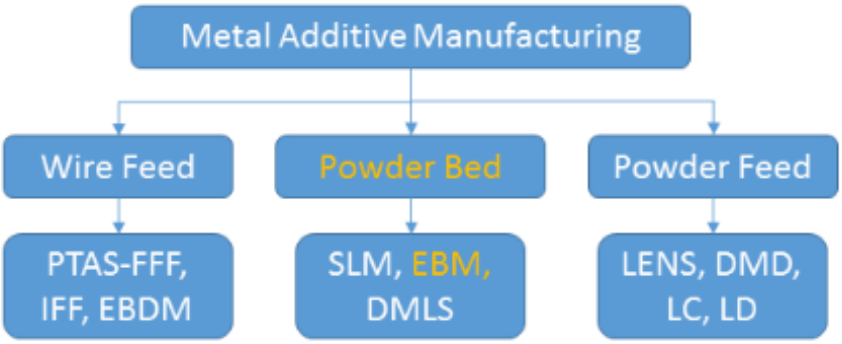

Figure 3. Hierarchical structure of metal AM, highlighting EBM's place in terms of material feedstock as well as a selection of processes that fall under each category.

Traditional metal machining (milling, turning, and cutting) starts with a block (billet) of material and removes the unwanted parts to produce an object. Traditional manufacturing methods such as casting, machining, pressing, and so on are well known and have been used for a long time. Metal AM, however, introduces a new and even more complex paradigm. The bulk material properties of the conventionally machined part are normally the same as that of the original billet. For better or worse, AM changes this, and the resulting product has material properties that may or may not significantly differ from those of the material put into the process.

3.1 Powder bed fusion

ISO/ASTM standard 52900:2015(E) [1] defines PBF as an "*Additive manufacturing process in which thermal energy selectively fuses regions of a powder bed*". A generic PBF process consists of a heat source (laser or electron beam) selectively melting layers of powder. For each layer, the powder bed (or part of the bed) is lowered, and new powder is deposited on the bed from a feedstock container by a powder deposition device, typically a roller or rake. The process repeats until the build is complete.

PBF processes are categorized into laser powder bed fusion (L-PBF) and electron beam powder bed fusion (EB-PBF), each of which has its own advantages and drawbacks. L-PBF generally has a better surface finish of parts, more available materials for processing, easier post-processing since the surrounding powder is not sintered, and the ability to process non-conductive materials. EB-PBF operates under vacuum at high temperatures, which leads to contamination-free parts with low residual stress [11], and has a higher productivity in terms of build rate and the allowance for stacking of parts in the build chamber. The electron beam can be deflected at speeds that allow for processing techniques not possible with a L-PBF system, such as multiple simultaneous melt pools[1] (multi spot).

For a long time, there was only one supplier of EB-PBF equipment aimed at industrial use: Arcam EBM (Gothenburg, Sweden). Today, Freemelt (Mölndal, Sweden) has made available an open source EB-PBF machine with a focus on materials research and development. In Asia, the Japanese Ministry of Economic, Trade and Industry (METI) has established the Technology Research Association for Future Additive Manufacturing (TRAFAM). The project includes three academic institutions and 29 companies such as JEOL (Tokyo, Japan). One goal of the project is the development of an EB-PBF machine. Chinese manufacturers Xi'an Sailong Metal Materials (Xi'an, Shaanxi, China) and QBEAM (Tianjin, China) both have equipment available for sale. Regarding L-PBF technology, there are numerous suppliers of industrial machines such as SLM Solutions (Lübeck, Germany), Renishaw (Gloucestershire, United Kingdom), EOS (Krailling, Germany), 3D Systems

[1] Recent L-PBF machines have used multiple laser sources to increase productivity by having multiple simultaneous melt pools, albeit in lower quantity.

(Rock Hill, USA), Concept Laser (Lichtenfels, Germany) and Trumpf (Ditzingen, Germany). EB-PBF will be referred to as EBM throughout the remainder of this thesis.

3.2 Electron beam melting

Arcam AB, based in Gothenburg, Sweden, introduced the EBM process to the market in 1997 [11]. Now being a part of General Electric, Arcam is still the largest supplier of equipment for industrial use. Several other companies have announced plans to bring an EB-PBF machine to the market, and a few have followed through, but others are still to make this a reality. The EBM process utilizes a high-energy electron beam to melt a powder feedstock into desired geometries based on a 3D CAD model. The use of an electron beam requires the material for processing to be electrically conductive, which means that only metallic materials have been used so far. Commercially available materials are grade 2 titanium, titanium alloy Ti6Al4V/Ti64Al4V ELI, ASTM F75 cobalt-chrome, and nickel alloy 718, and titanium aluminide TiAl. Research has been done into using several other materials such as tool steel H13 [12,13], copper [14–16], nickel alloy 625 [17], Rene 142 [18], and in recent years stainless steel 316L and 316LN [19–21]. Compared to L-PBF technologies, EBM seriously suffers in industrial competitiveness due to the low number of materials available for processing.

3.2.1 Process and hardware description

EBM equipment has many similarities to a scanning electron microscope (SEM), but is much more powerful. EBM utilizes an electron gun that accelerates electrons towards the powder bed using 60kV of voltage. The beam then passes through a series of three electromagnetic coils, acting as lenses, which correct the shape of the electron beam (astigmatism coil), and then focus (focusing coil) and deflect (deflection coil) it to melt and sinter the powder on top of the powder bed. The powder feedstock is held above the build table in two powder hoppers, one at each side of the build tank. The rake fetches powder from the powder slopes, which are formed by openings at the bottom of the hoppers, and distributes the powder across the build table. The build platform moves vertically along the z-axis, with each layer change moving the component being built, the surrounding powder, and the start plate downwards along with it (see Figure 4).

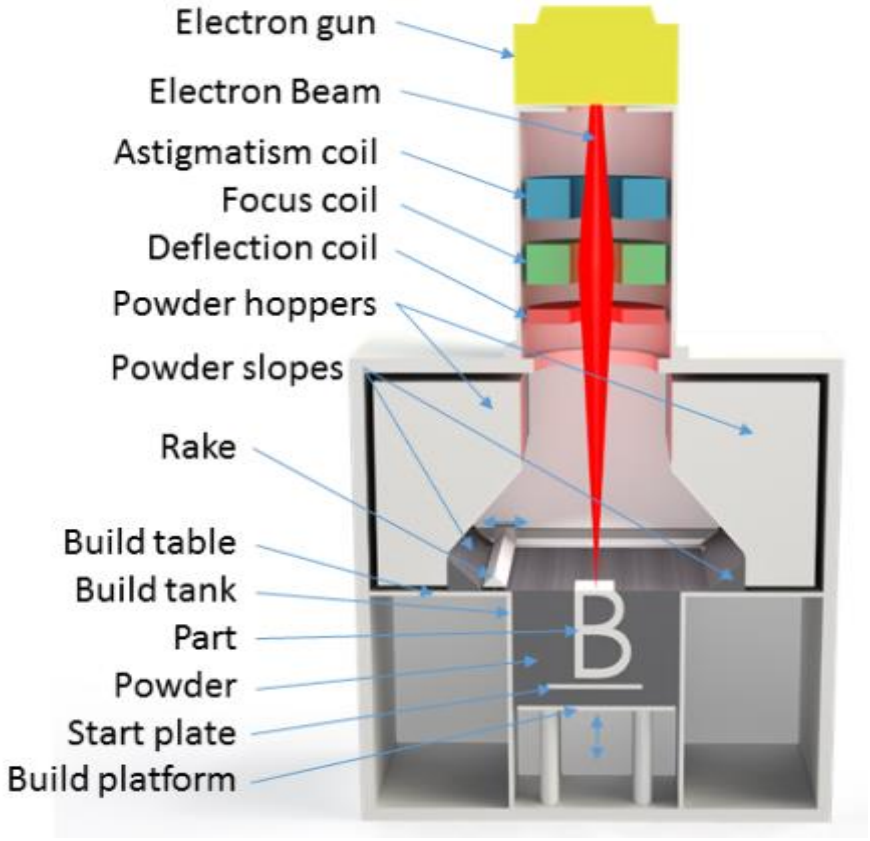

Figure 4. Cut-through simplified schematic of the Arcam EBM machine.

Figure 5 presents the EBM process as a 10-step flowchart.

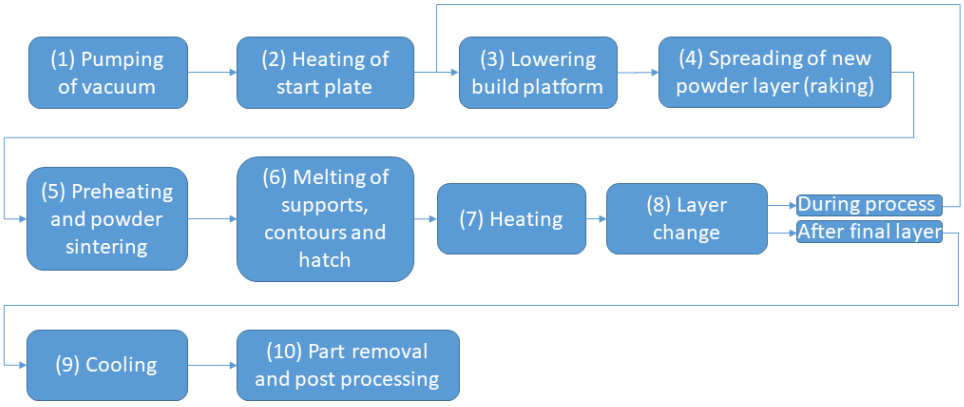

Figure 5. Flowchart of the EBM process.

(1) The process starts with removal of air from the build chamber and column. After air is pumped out, a small amount of helium is let into the chamber to regulate the pressure in the chamber to $2x10^{-6}$ Bar. Unlike air, helium is inert and does not cause unwanted reactions with warm metals, for instance oxidation. Low pressure is also a necessity to avoid collisions between the electrons in the electron beam and gas atoms while processing.

(2) Heating of the stainless steel start plate raises the temperature in the powder beneath the start plate and surrounding components, creating a heat buffer to stabilize build temperature. The plate is heated until a pre-set temperature is reached, typically between 700°C and 1050°C.

(3) The build platform is lowered to make room for the next layer. The platform descends into the build tank by the thickness of one layer, typically 50–150μm, and the start plate and surrounding powder descends with it. If a part is partially built, the part also descends. The lowering of the build platform means that the powder bed surface will always be at the same level throughout the build.

(4) The rake fetches powder from the powder slope and moves across the build table, filling the void created by the lowered build table with new powder.

(5) The newly deposited powder is preheated, causing a light sintering. Non-sintered powder has poor conductivity (imagine the theoretically infinitely small contact surface between two spheres). The electrons in the electron beam give a negative charge to the powder during interaction with the powder bed. Negatively charged powder grains repel each other, just like two similar ends of a pair of magnets. Since the powder has nowhere to go but up, this results in a cloud of loose powder filling the build chamber; a process-disruptive phenomenon known as smoke. Smoke is avoided by sweeping the electron beam over the new non-sintered powder at high speed with a large focus offset and long time between adjacent scan lines. This spreads the charge from the electrons and gives the still built up charge time to dissipate into the powder bed. It also creates enough heat to melt the powder grains in the powder bed slightly together (sintering), locking them into place and further reducing the charge build-up by increasing conductivity.

(6) After preheating and sintering, melting of powder without smoke is now possible. The geometry of the component is melted in a number of steps.

Typically first the supports, also known as wafers, are melted, and then the contours and finally the hatch (or bulk) material. However, the order is not fixed, and sometimes it could be beneficial to melt the bulk material first.

(7) After the melting steps, the heat model calculates if there is a need for more heat to maintain the build temperature. If so, a post-heating step is added in a similar way to preheating, with the electron beam sweeping the whole powder surface at high speed with a defocused beam. The beam is usually even more defocused than when pre-heating/sintering, in order to avoid further sintering which could cause problems with post-processing powder removal.

(8) One layer of the build is now completed. If there are more layers to add, the process jumps back to stage (3). If the just-completed layer was the final layer of the build, the process continues to step (9).

(9) The entire part is now built, but has a temperature of several hundred degrees Celsius. Letting air into the chamber at this stage could lead to contamination of both powder and component. One option is to let additional helium into the build chamber to increase the pressure and thereby speed up the cooling due to an increased convectional heat transfer. The cooling typically takes several hours.

(10) When the temperature reaches 100°C, the software allows the operator to ventilate the chamber with air to equalize the pressure, making it possible to open the build chamber door and extract the part. The component is then placed in the Arcam Powder Recovery System, which uses compressed air and the same powder as used inside the EBM machine as blasting media to remove the remaining coating of lightly sintered powder. The powder that is blasted free is then sieved, and can be reused in the EBM machine.

Aside from the heat source, it is the vacuum, preheating and sintering that primarily separates laser- and EBM-based PBF technologies. Because of the preheating, EBM usually applies an elevated process temperature, typically in the range of 700°C–1050°C. This elevated temperature results in a continuous heat treatment of the part to be built, facilitating microstructural grain growth and making the resulting component almost free from residual stress. The inputs and outputs of the EBM process are illustrated in Figure 6. What sets the EBM process apart from traditional machining is that the process itself has a significant impact on the resulting material properties and microstructure. If AM is used properly, this is beneficial, since it means a

material can be locally tailored to meet specific requirements of a component or even a certain part of a component [22–25]. This level of control also means

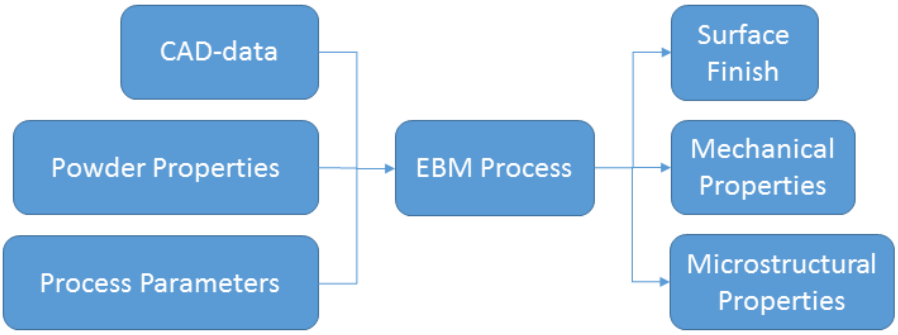

that the level of knowledge needed to design and manufacture parts using EBM is higher.

Figure 6. Flowchart describing the input and output parameters of the EBM process.

3.2.2 Process parameters

There are over 100 process parameters available for altering in the EBM Control 3.2 software used to control the modified Arcam S20 EBM machine for the experiments in this thesis [11]. It would be neither practical nor useful to list them all, but there are a few critical ones that need to be understood in order to control the process.

- **Beam speed (mm/s)** (beam deflection rate) is the speed at which the interaction point of the electron beam and the powder bed moves across the powder bed surface. Beam speed has a linear inverse effect on the energy input from the electron beam to the powder bed. Some sub-parameters also alter beam speed for certain specific occasions. One such occasion is "turning points" during hatching, which carry a risk of overheating the material as the beam changes direction at an edge and directly starts to melt new material right next to just-melted material. If the beam is speeded up for a certain distance before approaching and after leaving an edge, the energy input is lowered and local overheating is avoided.
- **Beam power (mA)** directly regulates the beam intensity. The EBM voltage is 60kV, and the beam power can be regulated between 0 and 50mA, which gives the EBM machine a power range of 0–3000W

(Power=Voltage×Current). Balancing beam speed and beam power is crucial to achieve the desired properties in the manufactured parts.

- **Speed function** includes both beam speed and beam power. This setting is a function that automatically compensates for differences in scan length for complex geometries by altering beam speed and power. Speed function was disabled in this thesis, since it alters parameters automatically without the direct control of the user.

- **Focus offset (mA)** determines the difference between the nominal current and the current passing through the middle coil in the column, which governs the beam focus. The nominal current is set as the current that results in the smallest spot size, meaning that a focus offset of 0 mA gives the smallest spot size. The effect of a non-zero focus offset is a translation of the focal point along the z-axis in the build chamber. This effectively alters the size of the interaction point between the electron beam and the powder bed, and thus alters the beam energy intensity on the powder bed surface. The focus offset is altered several times every layer during a build. The preheat stage, which includes interaction between the electron beam and non-sintered powder, uses a high focus offset value to lower the energy intensity and avoid smoke and unwanted melting of powder. Conversely, the melting steps require higher energy density and therefore a smaller spot size and lower parameter value.

- **Line offset (mm)** dictates the distance between adjacent scanlines. Like beam speed, line offset has an inverse linear effect on the energy put into the object to be built. A typical melt track has the shape of a half-circle with the flat part upwards. Spacing the melt tracks too close together (i.e. line offset too small; see Figure 7a) results in an excessive area energy and overheating of the material. Spacing the melt tracks too far apart (line offset too large; see Figure 7c) results in porosity in the cavity between the melt tracks. Figure 7b shows a good profile of melt tracks. A typical line offset is 0.05–0.2mm, but both larger and smaller values can be and have been used.

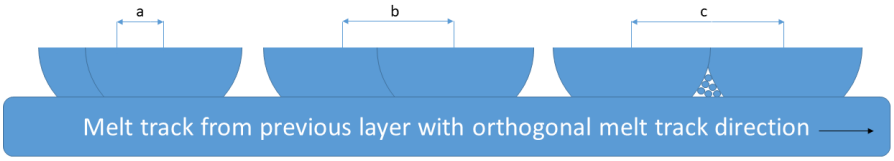

Figure 7. Three sets of melt track pairs; a, b, and c represent different line offsets.

- **Scanning strategy** has three main options: unidirectional, bidirectional (also known as snaking), and spot melting (Figure 8). Typically, unidirectional and bidirectional melting are used with hatch melting and spot melting is used with contours, but exceptions exist.

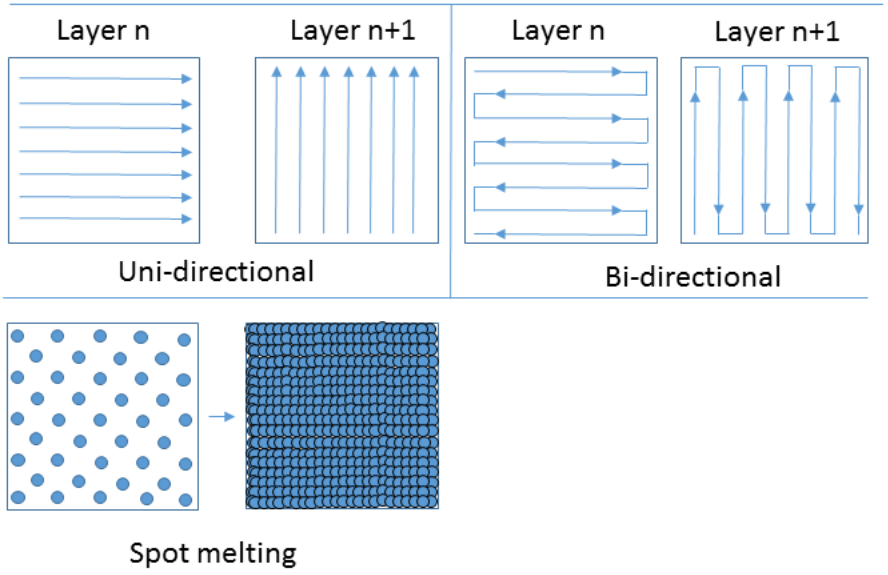

Figure 8. Different hatching strategies for the EBM process.

- **Layer thickness (mm)** determines how far the build table should lower with each layer change. Layer thickness is a tradeoff where thinner layers result in greater surface resolution for finer details in the z-direction, but also increase the number of layers needed to complete a build and thus increase the total build time. When varying the layer thickness, one usually has to alter the energy that goes into the powder bed to maintain a good melt. Thicker layers require more energy to preheat/sinter and melt.

When building complex structures, it is usually beneficial to use automatic functions, since they will likely produce good quality parts in a wide range of geometries. However, during process and material development the automation adds some uncertainty as to what parameters have really been used. To avoid uncertainties, automatic functions such as the heat model and speed function were deactivated during the work in this thesis.

3.3 Lightweight structures

When creating lightweight structures such as lattices, AM has a large advantage over traditional manufacturing. One application of lattices is their use in medical implants. The titanium alloy Ti6Al4V has been used for some time for implants in the human body. It has a higher elastic modulus than human bones, and this mismatch has been considered the reason for implants coming loose due to a phenomenon known as "stress shielding" [26]. One way to alleviate the issue is to design the implant with lattice parts tailored to match the mechanical properties of the surrounding bone tissue. This can be achieved by altering the type of lattice cells used and the thickness of the individual beams in the cells. Properties can be designed to be isotropic or anisotropic, rigid or ductile, and to have a controlled or collapsing compression behavior, among other options. The resulting lattice properties are determined by both the geometry of the lattice cells and the properties of the material from which the beams are made.

The two main types of lattices are reticulated mesh structures and stochastic foams [27,28]. Reticulated meshes consist of a unit cell which is multiplied to form a lattice structure. The selection of unit cell determines the lattice properties. Before AM, porous metallic materials were manufactured using various techniques such as powder metallurgy, metal foaming, and space holder methods [28], but these methods give only limited control of pore size, geometry, and distribution. AM, on the other hand, can produce the same pre-determined stochastic foam geometry as many times as needed.

3.4 Stainless steel for additive manufacturing

There are several ways to make powder for AM. The most common is gas atomization, where a batch of molten metal alloy is prepared by melting feedstock of each comprising element in the specified amount. The molten alloy is forced through a nozzle into the atomization chamber, where it is impinged with a gaseous medium (air, nitrogen, helium, or argon) and breaks into powder particles 0–500μm in size. Typical outcome for this method is mostly spherical particles with some asymmetrical particles and satellites. The powder is then sieved to contain only the desired fraction. Another process for making AM powder is plasma atomization. The principle is the same, but instead of a molten alloy being blasted by gas, a wire feedstock is fed into a plasma torch which atomizes the wire. Plasma atomization produces powder of a higher quality than gas atomization in terms of sphericity of particles. However, it is limited by the fact that the metal to be atomized must be

possible to form into a wire for feeding. Size range for plasma atomized powder particles is 0–200µm. There are several other methods for producing metal powders for AM, but gas and plasma atomization are the two most common.

Powder size range is not the only important factor in AM; the sphericity of the particles must also be considered. Figure 9 shows a 316LN powder used for EBM. Spherical particles are visible, and attached to some of them are much smaller particles, called satellites. Free particles in the size range of satellites are too small to be safely used, and are sieved away during the fabrication of the powder, but some attach to larger particles during atomization and end up in the powder batch anyway. Figure 9 also shows a number of non-spherical powder particles; these particles tend to affect the powder in terms of flowability, and if there are too many of them then problems may occur in the raking process at the start of each layer during a build.

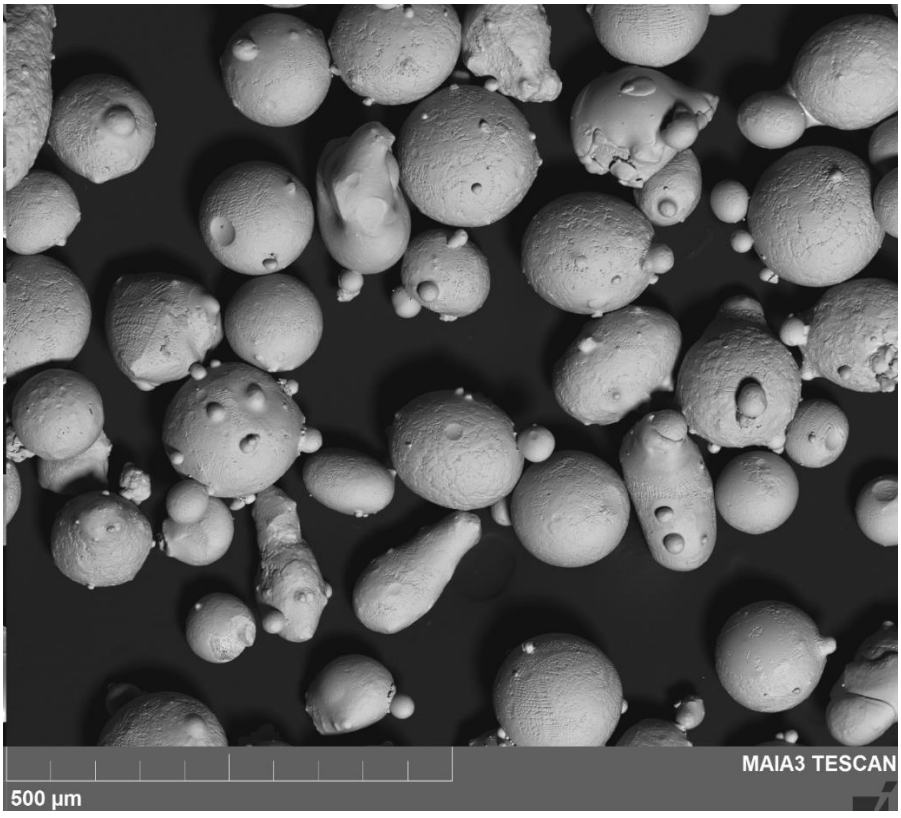

Figure 9. SEM image of 316LN powder, showing spherical particles, satellites, and non-spherical particles.

3.5 Alloy 316LN

Stainless steel 304 (EN 1.4301) and stainless steel 316 (EN 1.4401) are probably the most commonly used stainless steels. The only difference between them is the addition of ~2-3% molybdenum to 316. Molybdenum gives 316 a greater corrosion resistance against chloride and salt-containing environments such as seawater, which makes 316 a good choice for use in marine applications. Other applications for 316 include medical surgical instruments and industrial, food, and chemical processing equipment. Stainless steels must contain at least 10.5% of chromium to be called stainless. Additional alloying elements can be molybdenum, nickel, titanium, aluminum, copper, nitrogen, phosphorus, and selenium.

316L (EN 1.4404) differs from 316 in that it has a lower carbon content, which makes it less susceptible to carbide precipitation caused by high temperatures, known as sensitization, and hence more resistant to grain boundary corrosion after processes such as welding. 316LN (1.4406) is a nitrogen-enriched version of 316L. The addition of nitrogen provides additional resistance to sensitization in certain circumstances as well as some solution hardening, which slightly increases the minimum yield strength requirements compared to 316L. The elemental composition of 316LN according to ASTM A240 is presented in Table 1.

Table 1. The elemental composition requirements of 316LN according to ASTM A240/240M.

Element	Weight %
Carbon	0.030*
Manganese	2.00*
Phosphorus	0.045*
Sulfur	0.030*
Silicon	0.75*
Chromium	16.0–18.0
Nickel	10.0–14.0
Molybdenum	2.00–3.00
Nitrogen	0.10–0.16

* Maximum value

3.6 Build preparation

Before the build can take place, a stereolithography (.stl) file containing the desired geometry needs to be produced. Most computer-aided design (CAD) software can do this. For Papers 1 and 2, SolidWorks (Dassault Systèmes,

Vélizy-Villacoublay, France) was used to design the base geometry and Magics (Materialise, Leuven, Belgium) was used to prepare the .stl files for slicing. For Paper 3 only Magics was used, since the geometry was much simpler. When preparing a build file, all components are positioned in a virtual build tank, which corresponds in size to the actual build tank in the EBM machine. Next, the slicer software (Arcam Build Assembler) loads the .stl files and divides them into multiple thin layers, typically 50–200μm thick, corresponding to the layer thickness the EBM machine will later use when building the part. The output from the slicer is an Arcam Build File (.abf) which is loaded into the EBM machine. In the EBM machine, each .stl file within the .abf file is assigned a processing theme that governs how the electron beam will behave when melting that specific geometry. Unlike traditional machining, which is controlled by a pre-set program, the Arcam EBM machine uses real-time calculations to control the position of the electron beam on the powder bed. This makes it possible to control and alter process parameters while the machine is operating, a feature that is often used when developing process parameters for a new material.

4 Materials and methods

4.1 Material

The alloy 316LN was used throughout this work. Carpenter Powder Products AB (Torshälla, Sweden) supplied the precursor powder. Powder flowability was measured with a Hall flow funnel, and packing density was determined using a 10^{-4}g resolution scale. A modified Arcam S20 EBM machine was used to build all samples and tensile bars. The modifications included replacement of components in the build chamber, bringing it to a state where it closely resembled an Arcam A2 machine. The EBM machine was controlled with EBM Control 3.2 software. The layout of the lattice build for Papers 1 and 2 is presented in Figure 10, and the layout of tensile bars for Paper 3 is presented in Figure 11.

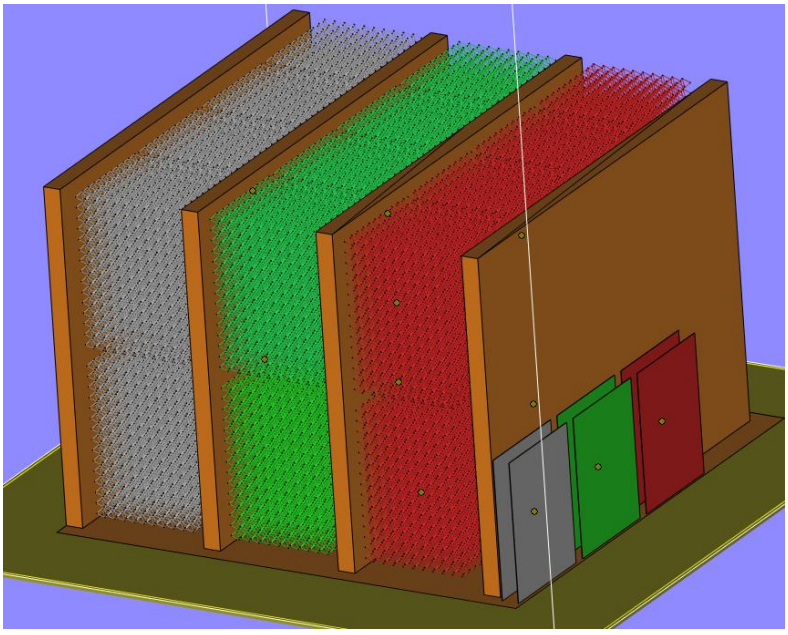

Figure 10. Placement of the lattice samples separated by the solid walls in the CAD file of the build generated by Magics software. Different colors represent different process settings.

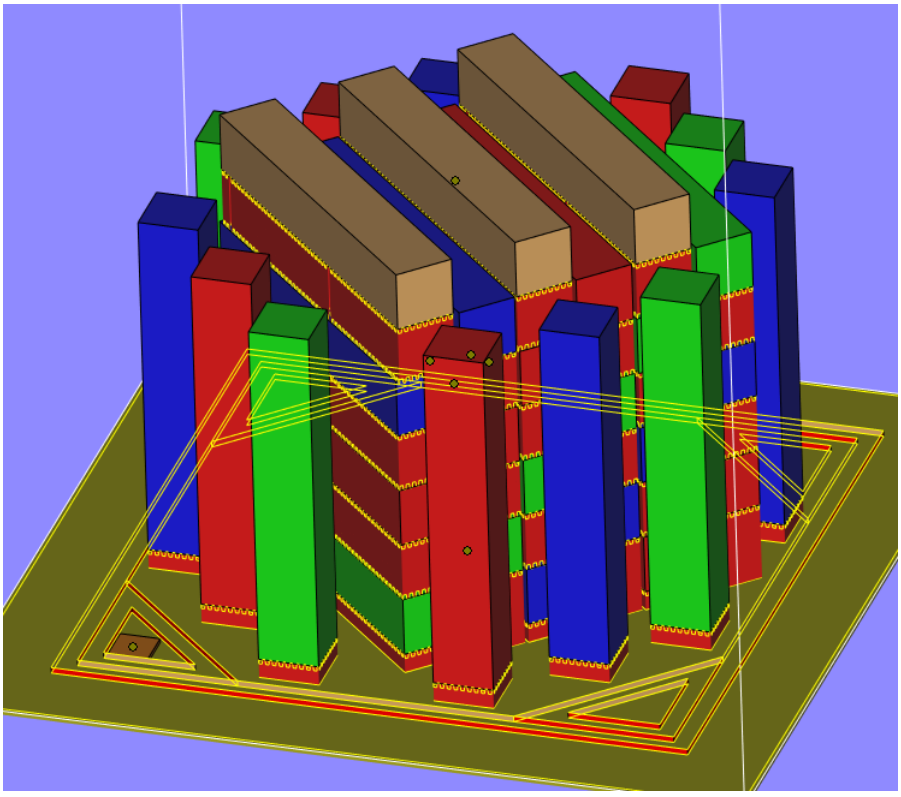

Figure 11. Placements of blocks for tensile rods. Different colors represent different process parameter settings.

4.2 Metallographic preparation

Specimens were prepared in order to reveal their microstructural features, in different ways according to the requirements of the different studies. The lattices in Papers 1 and 2 were encapsulated in epoxy resin for protection during the cutting and polishing process. Specimens were then ground from the top face using a 240 grit sand paper to obtain xy cross-sections (perpendicular to the building direction, z). Cross-sections were prepared by careful manual polishing using rotating diamond coated abrasive plates from 56µm down to 3µm. Subsequent polishing was performed using a rotating polishing cloth combined with 1 µm diamond paste and final polishing using a rotating cloth and colloidal silica suspension. Polished specimens were chemically etched using Kroll's reagent. A series of etching stages at increasing times in the range of 15 to 40 minutes with consecutive microscopy was performed to reveal different microstructural features.

For the solid specimens in Paper 3, the same grinding procedure was used. Since the solid samples were not at risk of breaking during grinding, some were encapsulated in epoxy resin and some were not. The reason for encapsulating some samples was due to increased effectiveness in polishing several samples at the same time as well as loading several samples simultaneously in the SEM. With a desire to move away from Kroll's reagent, which contains hazardous hydrofluoric acid, electrochemical etching was used for the solid samples using the 316LN sample as anode along with a platinum cathode, both submerged in an oxalic acid solution (saturated solution + 10 volume % distilled H_20). A voltage of 2V and no current limitation was applied for 30–60s, which revealed grains and sub grains.

4.3 Scanning electron microscopy and energy-dispersive x-ray spectroscopy

SEM was used in Papers 2 and 3 to capture images of microstructural features such as grain boundaries, grain boundary precipitates, granular substructure, and pores for both lattices and solid samples. The SEM was typically operated between 10kV and 30kV to reveal different features. Several different SEMs were used, including a Tescan Maia 3 and a Tescan MV2300VP (Tescan, Brno, Czech Republic). Energy-dispersive x-ray spectroscopy (EDS) equipment coupled to the Maia 3 SEM was used in Papers 2 and 3 to examine the elemental composition of the overall material as well as grain boundary precipitates.

4.4 Microstructural grain size

In all three papers, grain sizes were measured using ImageJ (National Institutes of Health, United States), an image analysis software package capable of particle analysis. The particle analysis function was used to count and determine the grain size of each grain in a SEM image. To assure correct detection of grain boundaries by ImageJ, the SEM images were manually improved by tracing the grain boundaries and converting the image to black and white.

4.5 Hardness measurement

Traditional hardness testing relies on a probe inserted into the sample to be tested. By using load and position data, it is possible to calculate the material's hardness. However, this is not an ideal method of testing lattice structures,

due to the flexibility of the structure and the fact that the probe is in the same size range as the object to be tested. In Paper 2, this problem was solved by nanoindentation, which applies the same principle but at a much smaller scale. It is now possible to take individual measurements separated by only a few μm, which means a series of measurements can be made at each individual lattice beam. The hardness measurements for Paper 3 were performed using a Mitutoyo HR200 machine.

4.6 Density measurement

The density of a material is determined by dividing its weight by its volume. Density measurement plays an important part in materials development, since it can reveal whether there is porosity inside a material that is supposed to be 100% solid. For the evaluation of lattice samples in Papers 1 and 2, the density measurement was not intended to find pores inside the beams themselves but rather to find out the air-to-steel ratio of the lattices. This was achieved by weighing the samples and dividing the weight by the measured outer dimensions of the lattice structure.

When processing metal powder via PBF into solid material, there is always some degree of porosity. For Paper 3, the interest lay in finding out whether there were any internal pores inside the nominally 100% solid steel cubes, and quantifying the total porosity volume as a percentage of the cube as a whole. Archimedes' principle states that the upward buoyant force exerted on a body immersed in a fluid, whether fully or partially submerged, is equal to the weight of the fluid that the body displaces, and acts in the upward direction at the center of mass of the displaced fluid. This principle can be expressed as:

$$\rho_{sample} = \frac{W_{in\ air} * \rho_{liq.}}{W_{in\ air} - W_{in\ liq.}}$$

where (ρ_{sample}) is the density of the object to be measured, $W_{in\ air}$ and $W_{in\ liq.}$ are the measured sample weights in air and liquid, and $\rho_{liq.}$ is the density of the liquid. By dividing the measured density by the theoretical 100% solid density, one gets the relative density.

4.7 Tensile testing

Tensile and compression testing were performed using an Instron 5969 Universal Testing System (Instron, USA) equipped with a clip-on extensometer. The ASTM E8 [29] and ISO 13314-2011 [30] standards were

followed to ensure comparability between studies. Specimen geometry for tensile testing in Paper 3 is presented in Figure 12.

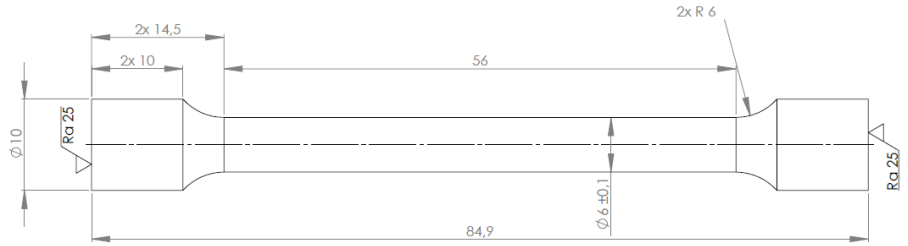

Figure 12. Dimensions of tensile specimens in compliance with ASTM E8.

4.8 Data processing and statistical methods

Data were processed and presented in terms of arithmetic mean and standard deviation. Standard deviation was determined using the n-1 method (Bessel's correction), where the standard deviation (s) is equal to $\sqrt{\frac{\sum_{i=1}^{n}(x_i-\bar{x})^2}{n-1}}$.

Statistical significance was set at $p<0.05$ (double sided).

Raw data were exported from the Bluehill 3 software controlling the Instron tensile testing equipment into a comma-separated text file (.csv), which was then imported into and processed in Microsoft Excel. Excel has shown poor performance when plotting larger datasets, and so due to the large quantity of data (10000+ datapoints) in some samples, Origin (OriginLab, Massachusetts, USA) was used for plotting data in Papers 1 and 2 while Veusz (Garching, Germany) was used in Paper 3.

5 Results

5.1 Paper 1

This paper discusses the possibility of manufacturing lightweight structures, such as lattices, in stainless steel 316LN. It is a direct response to RQ1, which asks if it is feasible to manufacture lightweight structures from a 316LN precursor powder via EBM.

Summary: EBM technology can successfully be used to fabricate lightweight lattice structures in 316LN stainless steel. The compression behavior differed from that of titanium. As shown in Figure 13, the ductility of 316LN and the shape of the lattice unit cells made the compression stress/strain curves smooth instead of the typical sudden drops in stress due to structural collapse, something that is often seen in lattices made from Ti6Al4V.

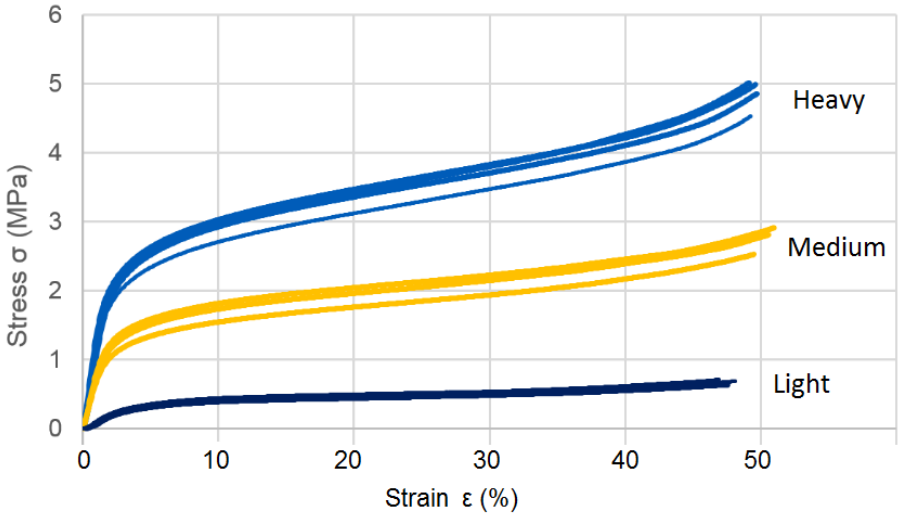

Figure 13. Stress/strain diagram from compression testing of 316LN octagon cell lattice structures fabricated using EBM technology. The relative density of the lattice structure is categorized as heavy (blue), medium (yellow), and light (black).

This study also showed that it is possible to alter the mechanical properties of the lattice structure by changing only the EBM process parameters, without altering the input CAD geometry. Table 2 shows the as-built weight and volumetric air-to-metal ratio of the different lattices, all manufactured using the same CAD geometry.

Table 2. Differences in EBM lattice samples with identical CAD geometry and varying process parameters.

Sample	Average weight (g) (SD)	Average dimension x × y × z (mm)	Average porosity (%)
Light	18.43 (0.24)	29.75 × 29.75 × 44.6	94.2
Medium	29.71 (0.26)	29.9 × 29.9 × 44.9	90.7
Heavy	37.73 (0.23)	30.0 × 30.0 × 44.9	88.3

5.2 Paper 2

Paper 2 continues the work from Paper 1 by looking into the microstructural properties of the EBM-fabricated lattices. This paper is a direct response to RQ2, but also relates to RQ1 in that if the microstructural properties do not meet the requirements then it could be argued that the manufacturing of lattices was unsuccessful.

Summary: The EBM-fabricated lattices showed a fine microstructure. When comparing the lattice microstructure to EBM-manufactured bulk material, the bulk material microstructure was of the order of 10 times coarser. The grains had a wide size range, with clusters of fine grains along the periphery of the beams (Figure 14). Furthermore, the EDS scan of bulk material of the lattice beam showed that the stainless steel material was within the ASTM A240 specification aside from a slightly too high level of chromium (0.05%); see Table 3.

Table 3. Elemental composition of various 316LN materials. EBM samples based on EDS analysis.

	Si (wt%)	**Cr (wt%)**	**Mn (wt%)**	**Ni (wt%)**	**Mo (wt%)**	**Fe (wt%)**
316LN (ASTM A240)	0–0.75	16–18	0–2	10–14	2–3	Bal.
Powder manufacturer spec.	0.5	17.6	1.7	12.3	2.46	Bal.
Lattice samples (EBM)	0.58	18.05	1.53	12.26	2.86	64.72
Lattice sample precipitate (EBM)	1.09	29.74	-	5.18	12.13	51.86
Bulk material (EBM)	0.53	17.4	1.5	12.4	2.5	Bal.

Table 3 and Figure 15 also show how the grain boundary precipitates were rich in chromium and molybdenum while completely lacking manganese.

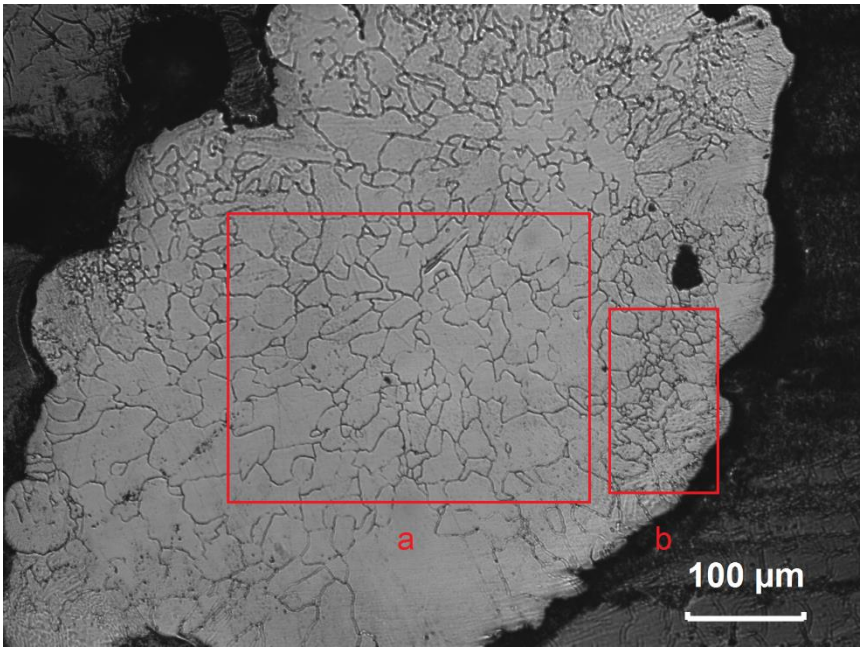

Figure 14. Typical lattice strut cross-section normal to the build direction. Boxes (a) and (b) highlight differences in grain size depending on location in the strut cross section. Average grain area was 435µm^2 for the inner parts of the cross-section (a) and 95µm^2 for the periphery (b).

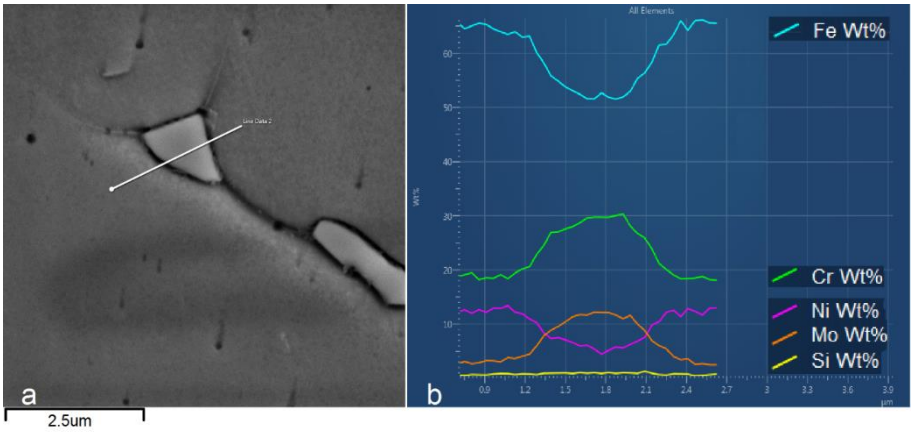

Figure 15. Line EDS scan of grain boundary precipitate (a) showing increased levels of chromium, molybdenum, and silicon (b).

The size of the sub-grains ranged from 1µm to 5µm, which is about twice as large as the 0.5–2µm size range in the bulk material. It was also found that the

typical elongation of grains along the building direction did not occur in the case of lattices; instead, the grains were elongated along the beams, which were angled at ~55 degrees from the build direction (Figure 16).

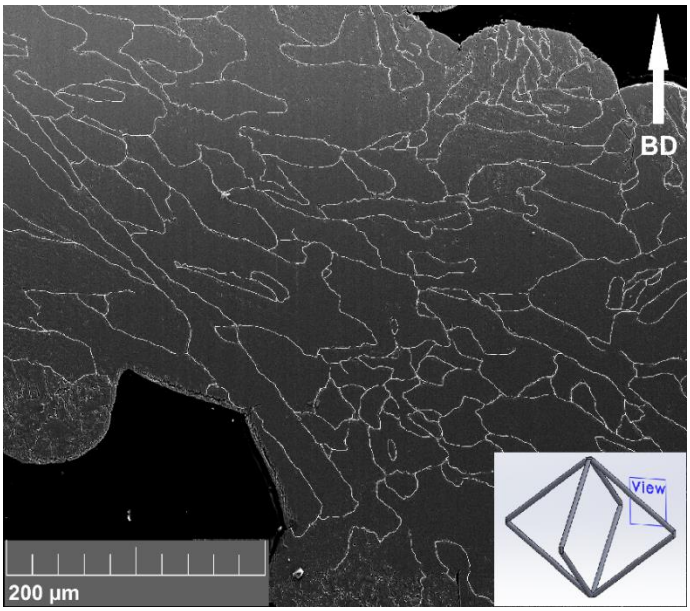

Figure 16. Typical cross-section of the lattice strut with the cut plane along the strut axis (insert shows the cross-section area in the lattice cell), illustrating the predominant elongation axis of the grains.

5.3 Paper 3

Paper 3 focuses on EBM fabrication of bulk material in 316LN stainless steel. It develops a process window, and examines mechanical and microstructural properties of test samples manufactured within different parts of this process window. This paper answers not only RQ3 but also the overall question regarding a process window for 316LN bulk material.

Summary: Sample cubes were manufactured using a wide variety of beam speeds and energy inputs. A process window was defined by examining the top surfaces and determining the porosity via Archimedes' principle (Figure 17).

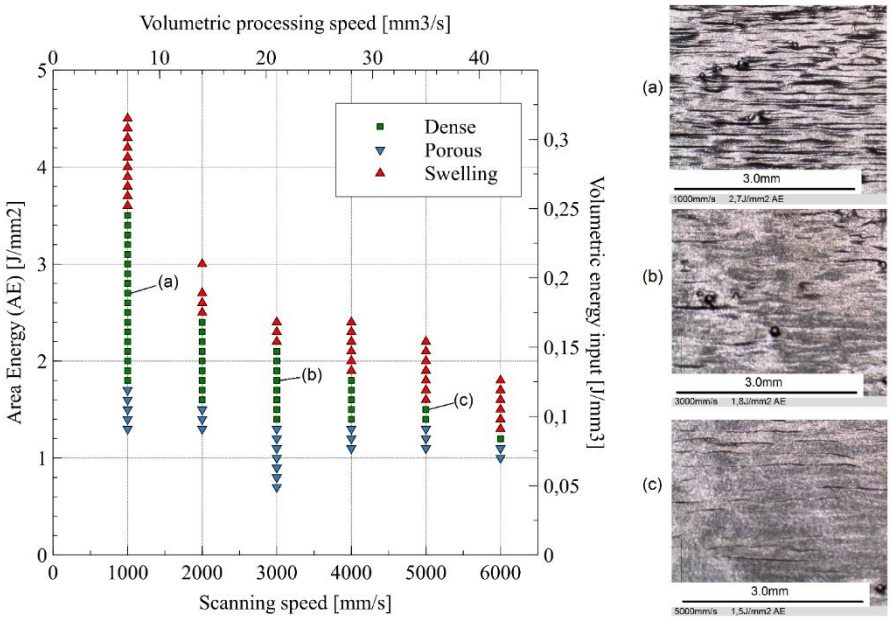

Figure 17. Process window for EBM-processed 316LN stainless steel at 70μm layer thickness and 0.1mm line spacing. (a), (b), and (c) show the top surfaces of specimens and their respective positions in the process window. For ease of comparison to other process development studies, volumetric energy (accounting for layer thickness) and volumetric processing speed have been added as secondary axes.

Three sets of parameters (a, b, and c in Figure 17) were chosen from the process window, and tensile bars were manufactured to determine the mechanical tensile properties. The tensile tests confirmed the well-reported anisotropic behavior of additively manufactured material, with strength along the build direction (z) lower than in the xy direction (Figure 18 and Table 4). Higher deflection speeds of the beam resulted in lower elongation before break and lower apparent density.

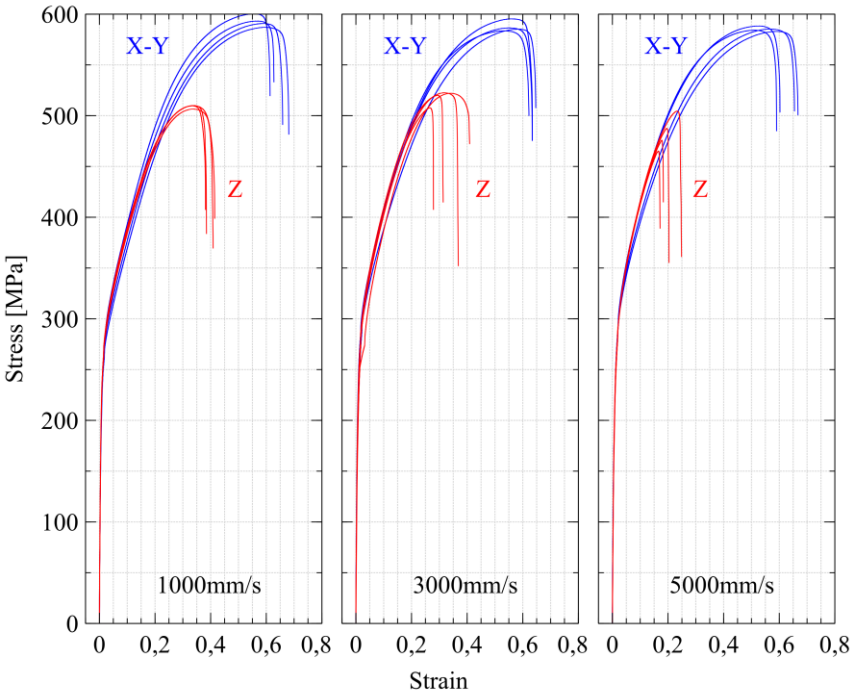

Figure 18. Tensile test results of EBM-built 316LN stainless steel bars processed with deflection speeds of 1000mm/s, 3000mm/s, and 5000mm/s.

Table 4. Test results (yield and ultimate tensile strength) of 316LN stainless steel processed via EBM in terms of arithmetic mean ± standard deviation (n-1).

EBM-built samples	YS (MPa)	UTS (MPa)	Elongation (%)*
xy 1000mm/s	271.3 ± 7.8	592.7 ± 5.5	63.2 ± 2.2 / 72.4 ± 4.3
xy 3000mm/s	284.2 ± 4.6	587.4 ± 5.2	63.5 ± 1.7 / 75.0 ± 0.0
xy 5000mm/s	290.1 ± 5.9	585.2 ± 2.4	62.2 ± 3.9 / 78.1 ± 2.1
z 1000mm/s	262.4 ± 2.5	508.9 ± 1.7	40.2 ± 2.6 / 39.6 ± 8.8
z 3000mm/s	273.0 ± 3.3	518.1 ± 7.0	34.5 ± 5.5 / 35.9 ± 9.2
z 5000mm/s	279.4 ± 1.6	483.2 ± 16.7	20.0 ± 4.0 / 16.7 ± 3.8
ASTM A743M (cast)	205	515	40***
ASTM A276 (wrought)	255	515**	35***
ASTM F3184 (AM)	205	515	30

** Values are post-test measurements for gauge lengths 50 mm and 24 mm respectively*

*** Annealed, thickness > 12.7mm (1/2")*

**** Gauge length = 50mm*

With statistical significance set at $p<0.05$ (double-sided), changes in beam deflection rates and area energies produced no significant differences in tensile properties in the xy direction. In the z-direction, going from 1000mm/s and 2.7J/mm^2 to 5000mm/s and 1.5J/mm^2 produced a higher yield strength but lower elongation. Even with $p<0.05$, there was no significant difference between 1000mm/s and 3000mm/s or between 3000mm/s and 5000mm/s, nor was there a significant difference in ultimate tensile strength.

6 Discussion and conclusion

6.1 Comments on materials and methods

It is clear from Papers 1 and 2 that the lattice properties can be modified by changing process parameters alone, without altering the CAD geometry. However, there are several strategies for building lattices, all of which are likely to have different results. Papers 1 and 2 explored one strategy that involved building an actual 3D CAD geometry of the lattice. Using this strategy for larger lattices with the same software as in these papers is not feasible, since the low frame rate and high loading times made it difficult to work with the resulting mesh. There is software that uses one-dimensional elements instead of three-dimensional, which is likely to lighten the computational load and make the models easier to work with. However, the use of one-dimensional elements has not yet been tested and it is unclear whether the Arcam software can interpret such models for use in the EBM machine. In Papers 1 and 2 the energy input into each lattice beam was controlled by contour melting parameters. Using the same strategy with one-dimensional beams will not be possible, and so there is a need to develop a new strategy, possibly a new kind of theme, for controlling the energy input.

The resulting process window in Paper 3 was developed on the basis of producing nearly a hundred 15x15x15mm^3 cubes, and yet they only represent the variation of beam deflection rate and area energy. To explore every parameter combination (focus offset, layer thickness, hatching strategy, line offset, and so on) to the same extent, one would need to fabricate 100^n test pieces (where n is the number of parameters in the test). With only the parameters mentioned, this would result in hundreds of millions of test cubes and the need for a 6-dimensional way of describing the results, which of course is not feasible. Not every parameter is reasonable to alter in so many steps, so in reality the required number of cubes is lower than hundreds of millions, but still in the range of tens of thousands.

Previous studies at the Sports Tech Research Center have used an overall strategy of high power, low deflection rate, and large line offset, resulting in material with excellent ductile properties; however, the processing speed has suffered. The present work explored the effects of increased processing rate

on the material properties. The strategy used for determining the process window was to fix a large number of parameters according to prior experience (from working with similar materials) of what is likely to work, including 5mA focus offset (small spot size), 70μm layer thickness, snaking, and 0.1mm line offset. Good industrial productivity is not the only reason for trying to go as fast as possible. With lower deflection speed, the layer times can be so long that the machine is incapable of completing a tall build with many parts in it because of the limited lifetime of the filament in the electron gun. To replace the filament, one must let the build cool, repressurize the build chamber, replace the filament, depressurize the chamber again, and restart the process (if possible). This is less of an issue for Arcam Q-series machines or newer, since they utilize a different technology for the filament with ten times the longevity of earlier versions.

Accurately quantifying material porosity is one of the hardest tasks in characterization, and is a common topic of discussion at conferences. Relative comparisons between different samples can be made fairly easily, for example by using Archimedes' method, but problems arise when there is a desire to accurately quantify porosity. A large number of parameters need to be controlled, and while some are easily handled (temperature of liquid and weight of sample) others are harder to deal with, such as how well the sample is wetted, and ensuring that there are no bubbles of air attached to the sample which would cause buoyancy and skew the measurement. Moreover, Archimedes' principle does not account for open pores located at the surface, since under ideal conditions the liquid would fill these pores and thus exclude them from the measurement. Wetting can be improved by using a wetting agent to reduce surface tension, but this is not a complete fix, and the exclusion of surface porosity is something one must simply bear in mind and accept.

Other methods for determining porosity include:

- Optical quantification
- X-ray computed tomography (X-ray CT)
- Gas pycnometry
- Mass/volume calculation

Optical quantification involves cutting and polishing samples and optically determining the porosity via a microscope. This method is heavily influenced

by the selection of cross-sections to examine, and the sample preparation is time consuming.

X-ray computed tomography is a rather expensive way of determining porosity, in comparison to Archimedes' method. The resolution drops as the size of the specimen increases, meaning that it is hard to accurately quantify porosity consisting of small (micrometer sized) pores in large volumes of material. However, this is probably the most accurate method for determining pores in a sample.

Gas pycnometry uses a gas instead of the liquid that is employed in Archimedes' method. The gas is either moved between chambers of known volume or pressurized in controlled ways in order to determine the volume of the sample in the chamber. This method is more precise than Archimedes' method, since the problem with wetting of the sample is removed.

The mass/volume approach is the simplest method, performed by measuring the mass with a scale and dividing it by the ideal volume of the sample. The biggest uncertainty lies in the relation between theoretical and actual volume of the sample. One strength is that distribution of pores is irrelevant to the results. Gas pycnometry and Archimedes' principle offer ways to refine the results of mass/volume by measuring the sample volume instead of using a theoretical volume.

EDS also has its limitations. Lighter elements are hard to detect, and several elements may be hard to distinguish from one another because the emitted x-rays have similar characteristics. A given element may emit x-rays with several different energy levels, depending on beam energy and the electron shell configuration, which manifests as one element being responsible for several detected peaks. One should also be aware that even if the spot size is in the nm (imaging resolution) range, the interaction volume generating x-rays for EDS is in the μm^3 range. The interaction volume can be reduced by lowering the acceleration voltage of the electron gun, but this will also reduce the number of elements that can be detected, since the energy level of the emitted electrons will be insufficient to generate an x-ray to detect.

Tensile testing by either compressing lattices or stretching rods also has some factors which affect the results. The lattices in this thesis tended to swell under compression, meaning that the contact perimeter between the anvil and the lattice changed and a sliding motion occurred between anvil and lattice. One could argue that this impacts the compressional stress/strain relationship,

since a counterforce is introduced in the beams from the friction forces in this sliding motion. However, the compression testing was carried out according to ISO 13314-2011, which ensures comparability to other studies despite this uncertainty.

The main uncertainty in tensile testing of solid rods is the accuracy of strain values. The initial 5% strain of the tensile testing is measured with a high resolution extensometer (Figure 19a) to accurately find the yield stress by only measuring a pre-defined section of the sample; this also eliminates any error from the grips settling under tension or slipping of the sample. For strains of 5% and above the built-in positioning system of the machine is used. Even if this positioning system has good resolution, the removal of the extensometer causes a discrepancy due to the inclusion of additional test sample geometry consisting of the remaining parts of the narrow section (the part outside the 50mm measured by the extensometer), the transition to the thicker parts, and the thicker parts themselves. The original gauge length of 50mm has now increased to the size of the whole sample (see Figure 19a and Figure 19b), and the geometry is inconsistent. The final elongation (maximum strain) of the sample is measured by placing the two broken tensile rod pieces together and measuring the distance between the spots, thus excluding the error caused by the geometry shift. For plotting the graphs from raw data, a compensation factor was introduced (measured elongation / raw data elongation) to make the graphical representation concur with the values presented in Table 4.

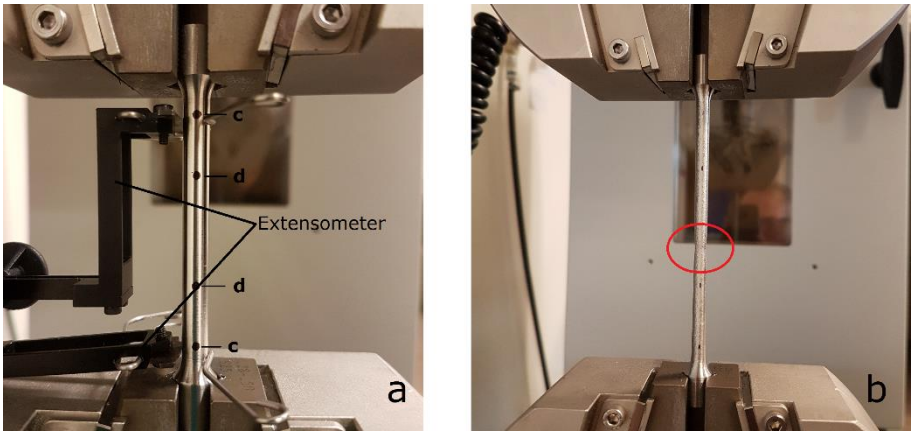

Figure 19. Tensile bar at test start (a) and with extensometer removed (b). The red circle in b highlights the necking area just before break. Dots at c and d in (a) are markings for post testing of final elongation; distances c-c = 50mm and d-d = 24mm.

Testing standard ASTM E8 dictates a gauge length of 24mm for the selected sample geometry, while material standards ASTM A743M, ASTM A276, and

ASTM F3184 specify that elongation values should be determined using a gauge length of 50mm. ASTM E8 allows for lengthening of the reduced (narrow) section to accommodate different extensometer sizes as long as the gauge length is retained. Thus, the testing complied with all mentioned standards by measuring the final elongation at both 24mm and 50mm distance (c-c and d-d in Figure 19a). A problem was encountered during the testing when the necking (where most of the final elongation takes place before break) occurred outside the 24mm area, causing irregular measurements in some samples (lower elongation before break). This was only the case for two of the 5000mm/s z-direction rods.

6.2 Comments on results

When the tensile results were compared with reported results from both EBM samples manufactured with the same machine as the Paper 3 samples [31,32] and samples manufactured using L-PBF [32,33], the ultimate tensile strength was approximately the same (~500MPa) in the Paper 3 samples and the referenced EBM samples, while the L-PBF samples had higher ultimate tensile strength (~600MPa). Yield strength in Paper 3 was slightly higher than in the referenced EBM samples (~275MPa vs. 253MPa), while yield strength in the L-PBF samples was almost twice as high (~490MPa). This is likely due to the Hall–Petch strengthening effect, which states that grain has a pinning point effect on dislocations with a direct effect on a material's ability to deform via dislocations. Smaller grain size (L-PBF) means more grain boundary pinning points and a higher yield strength, as described above. EBM-processed materials undergo a constant heat treatment during the process; the grains have time to grow, and are therefore comparatively large compared to L-PBF-processed material.

In terms of elongation, the EBM-built samples in Paper 3 had a lower elongation before break than both the referenced EBM samples (~58%) and the L-PBF samples (~48%). Elongation differed greatly between the build direction (20–40%) and the xy direction (~63%). A higher beam deflection rate yields a smaller average grain size, which increases the yield strength in the build direction, but the increase is not proportionate (from 262MPa to 279MPa) to the decrease in elongation before break. Ultimate tensile strength is important in some cases, but for most applications the stresses are not allowed to reach higher than the yield strength and often there is a safety factor that can be as great as tenfold. With this in mind, yield strength is the most

important tensile parameter. Regarding this aspect, EBM-processed 316LN stainless steel has some way to go before being able to compete with L-PBF-processed 316L stainless steel.

6.3 Future work and implications

The top surface can be considered representative of how each layer beneath looked after it had been melted. A smooth, pore-free top layer means a high likelihood of good-quality layers below. However, even if the top surface quality is good, there is still room for improvement. Varying focus offset and line spacing has the potential to increase top surface quality even further. In the interest of being productive, it would be worth exploring the effect of several different settings to improve the high deflection rate performance and increase the usable range of area energies to have some margins and increased robustness. More important, though, would be to look at ways to process the material to reach the yield strength of L-PBF-processed 316L.

6.4 Conclusion

Additive manufacturing using EB-PBF offers the potential for manufacturing parts of high quality in series production, but the technology is held back by the current shortage of available materials for processing. Stainless steel 316LN is a material with a wide range of industrial applications. This thesis has taken a first step towards introducing 316LN as a viable material for EBM commercialization, by showing that it is possible to manufacture, and alter properties of lightweight lattices, further exploring the process window for bulk material, and examining the material properties of samples from different parts of the process window.

7 References

[1] ISO/ASTM 52900:2015(E), Additive manufacturing — general principles — terminology (2015).

[2] J.E. Blanther, Manufacture of contour relief-maps, U.S. Patent No. 473901 (1892).

[3] Y. Zhai, D.A. Lados, J.L. LaGoy, Additive manufacturing: making imagination the major limitation, *JOM* (2014), 66, 808–816. doi:10.1007/s11837-014-0886-2.

[4] O.J. Munz, Photo-glyph recording, U.S. Patent No. 2775758 (1956).

[5] W.K. Swainson, Method, medium and apparatus for producing three-dimensional figure product, U.S. Patent No. 4041476 (1977).

[6] A. Ciraud, Process and device for the manufacture of any objects desired from any meltable material (1972).

[7] R.F. Householder, Molding process, U.S. Patent No. 4247508 (1981).

[8] H. Kodama, Automatic method for fabricating a three-dimensional plastic model with photo-hardening polymer, *Review of Scientific Instruments* (1981), 52(11), 1770–1773.

[9] J.A. Herbert, Solid object generation, *Journal of Applied Photographic Engineering* (1982), 8, 185–188.

[10] W.E. Frazier, Metal additive manufacturing: a review, *Journal of Materials Engineering and Performance* (2014), 23, 1917–1928.

[11] J. Karlsson, Optimization of electron beam melting for production of small components in biocompatible titanium grades, Doctoral thesis, comprehensive summary, Acta Universitatis Upsaliensis (2015). http://urn.kb.se/resolve?urn=urn:nbn:se:uu:diva-236709 (accessed November 21, 2014).

[12] D. Cormier, O. Harrysson, H. West, Characterization of H13 steel produced via electron beam melting, *Rapid Prototyping Journal* (2004), 10, 35–41. doi:10.1108/13552540410512516.

[13] L.-E. Rännar, A. Glad, C.-G. Gustafson, Efficient cooling with tool inserts manufactured by electron beam melting, *Rapid Prototyping Journal* (2007), 13, 128–135. doi:10.1108/13552540710750870.

[14] P. Frigola, O.A. Harrysson, H.A. West, R.L. Aman, J.M. Rigsbee, D.A. Ramirez, L.E. Murr, F. Medina, R.B. Wicker, E. Rodriguez, Fabricating copper components with electron beam melting, *Advanced Materials & Processes* (2014), 172, 20–24.

[15] M.A. Lodes, R. Guschlbauer, C. Körner, Process development for the manufacturing of 99.94% pure copper via selective electron beam melting, *Materials Letters* (2015), 143, 298–301. doi:10.1016/j.matlet.2014.12.105.

[16] R. Guschlbauer, S. Momeni, F. Osmanlic, C. Körner, Process development of 99.95% pure copper processed via selective electron beam melting and its mechanical and physical properties, *Materials Characterization* (2018), 143, 163–170. doi:10.1016/j.matchar.2018.04.009.

[17] L. Murr, S. Gaytan, D. Ramirez, E. Martinez, J. Hernandez, K. Amato, P. Shindo, F. Medina, R. Wicker, Metal fabrication by additive manufacturing using laser and electron beam melting technologies, *Journal of Materials Science & Technology*, (2012), 28, 1–14. doi:10.1016/S1005-0302(12)60016-4.

[18] L.E. Murr, E. Martinez, X.M. Pan, S.M. Gaytan, J.A. Castro, C.A. Terrazas, F. Medina, R.B. Wicker, D.H. Abbott, Microstructures of Rene 142 nickel-based superalloy fabricated by electron beam melting, *Acta Materialia* (2013), 61, 4289–4296. doi:10.1016/j.actamat.2013.04.002.

[19] L.-E. Rännar, A. Koptyug, J. Olsén, K. Saeidi, Z. Shen, Hierarchical structures of stainless steel 316L manufactured by electron beam melting, *Additive Manufacturing* (2017), 17, 106–112. doi:10.1016/j.addma.2017.07.003.

[20] J. Olsén, Z. Shen, L. Liu, A. Koptyug, L.-E. Rännar, Micro- and macro-structural heterogeneities in 316L stainless steel prepared by electron-beam melting, *Materials Characterization* (2018), 141, 1–7. doi:10.1016/j.matchar.2018.04.026.

[21] C. Wang, X. Tan, E. Liu, S.B. Tor, Process parameter optimization and mechanical properties for additively manufactured stainless steel 316L

parts by selective electron beam melting, *Materials & Design* (2018), 147, 157–166. doi:10.1016/j.matdes.2018.03.035.

[22] W. Xu, E.W. Lui, A. Pateras, M. Qian, M. Brandt, In situ tailoring microstructure in additively manufactured Ti-6Al-4V for superior mechanical performance, *Acta Materialia* (2017), 125, 390–400. doi:10.1016/j.actamat.2016.12.027.

[23] P.A. Morton, J. Mireles, H. Mendoza, P.M. Cordero, M. Benedict, R.B. Wicker, Enhancement of low-cycle fatigue performance from tailored microstructures enabled by electron beam melting additive manufacturing technology, Journal of Mechanical Design. 137 (2015). doi:10.1115/1.4031057.

[24] A.R. Balachandramurthi, J. Olsson, J. Ålgårdh, A. Snis, J. Moverare, R. Pederson, Microstructure tailoring in electron beam powder bed fusion additive manufacturing and its potential consequences, *Results in Materials* (2019), 1, 100017. doi:10.1016/j.rinma.2019.100017.

[25] M.M. Kirka, P. Nandwana, Y. Lee, R.R. Dehoff, Solidification and solid-state transformation sciences in metals additive manufacturing, *Scripta Materialia* (2017), 135, 130–134. doi:10.1016/j.scriptamat.2017.01.005.

[26] X.Y. Cheng, S.J. Li, L.E. Murr, Z.B. Zhang, Y.L. Hao, R. Yang, F. Medina, R.B. Wicker, Compression deformation behavior of Ti–6Al–4V alloy with cellular structures fabricated by electron beam melting, *Journal of the Mechanical Behavior of Biomedical Materials* (2012), 16, 153–162. doi:10.1016/j.jmbbm.2012.10.005.

[27] D.A. Ramirez, L.E. Murr, S.J. Li, Y.X. Tian, E. Martinez, J.L. Martinez, B.I. Machado, S.M. Gaytan, F. Medina, R.B. Wicker, Open-cellular copper structures fabricated by additive manufacturing using electron beam melting, *Materials Science and Engineering: A* (2011), 528, 5379–5386. doi:10.1016/j.msea.2011.03.053.

[28] D. Mahmoud, A.M. Elbestawi, Lattice structures and functionally graded materials applications in additive manufacturing of orthopedic implants: a review, *Journal of Manufacturing and Materials Processing* (2017), 1, 13. doi:10.3390/jmmp1020013.

[29] ASTM E8/E8M-13a, Standard test methods for tension testing of metallic materials (2013).

[30] ISO 13314:2011(E), Mechanical testing of metals — ductility testing — compression test for porous and cellular metals (2011).

[31] Y. Zhong, L.-E. Rännar, L. Liu, A. Koptyug, S. Wikman, J. Olsen, D. Cui, Z. Shen, Additive manufacturing of 316L stainless steel by electron beam melting for nuclear fusion applications, *Journal of Nuclear Materials* (2017), 486, 234–245. doi:10.1016/j.jnucmat.2016.12.042.

[32] Y. Zhong, L.-E. Rännar, S. Wikman, A. Koptyug, L. Liu, D. Cui, Z. Shen, Additive manufacturing of ITER first wall panel parts by two approaches: selective laser melting and electron beam melting, *Fusion Engineering and Design* (2017), 116 24–33. doi:10.1016/j.fusengdes.2017.01.032.

[33] Y. Zhong, L. Liu, S. Wikman, D. Cui, Z. Shen, Intragranular cellular segregation network structure strengthening 316L stainless steel prepared by selective laser melting, *Journal of Nuclear Materials* (2016), 470, 170–178. doi:10.1016/j.jnucmat.2015.12.034.